

Measure of high contact angles

Auriane Huyghues Despointes, Alice Mougey & David Quéré

*Physique et Mécanique des Milieux Hétérogènes, UMR 7636 du CNRS,
PSL Research University, ESPCI-Paris, France.*

Supplemental information

Here we complete our paper with a few supplemental figures, texts and toolbox that mainly discuss our methods and its accuracy, together with the degree of adhesion of the drops.

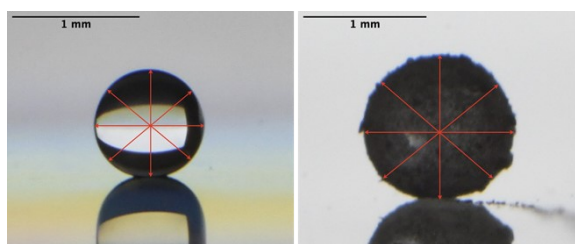


Figure S1. Measurement of the average radius of a pearl or a marble. The diameter $2R$ of the droplet is determined as the mean of the four red-marked segments in the image, for a water pearl with $2R = 0.85 \pm 0.01$ mm and a water marble with $2R = 1.19 \pm 0.02$ mm. The uncertainty is given by the dispersion of these measurements and it is reported in figures 2 and 3 of the accompanying paper.

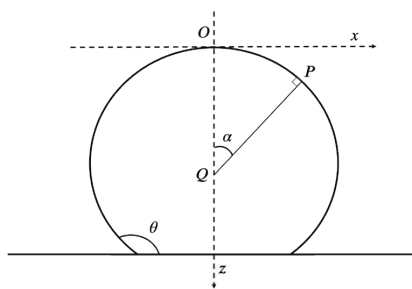


Figure S2. Integration of the Laplace Equation. Definition of the parameters used to integrate the Laplace equation for a hydrophobic drop.

We consider a droplet (surface tension γ and density ρ) with contact angle θ on a hydrophobic solid (figure S2). Its shape results from a balance between capillary forces and weight. Let P be an arbitrary point at the surface. The drop is axisymmetric and its main curvature radii are μ in

the plane of the figure, and the distance PQ (defined in the figure) in the perpendicular direction. On the one hand, we have $\mu = ds/d\alpha$, where s is the curvilinear abscissa and α is the latitude of point P . On the other hand, we have $PQ = x/\sin\alpha$, where x is the abscissa of point P .

The Laplace pressure inside the drop is $\Delta P = \gamma/\mu + \gamma/PQ$. In addition, the hydrostatic pressure can be written $\Delta P(z) = 2\gamma/r + \rho gz$, where the radius of curvature at the North pole of the drop is r , whose value is deduced from volume conservation. Introducing the capillary length $\kappa^{-1} = (\gamma/\rho g)^{1/2}$, and the relationships $dx = ds \cos\alpha$ and $dz = ds \sin\alpha$, the pressure balance leads to the equilibrium equations $dz/d\alpha = \tan\alpha dx/d\alpha$ and $dx/d\alpha = r \cos\alpha / (2 + z r \kappa^2 - r \sin\alpha/x)$. The latter equation is integrated for α between 0 and θ , taking as a boundary condition $\sin\alpha/x = 1/r$ for $\alpha=0$ and $x=0$. Hence, we get the complete theoretical shape of the drop, from which we can extract the contact size $2l$ (figure S3), which provides us with the fits drawn with dotted lines in Figures 2 and 3 of the accompanying paper. The corresponding algorithm is given in the supplemental materials available on the journal site (python drop file).

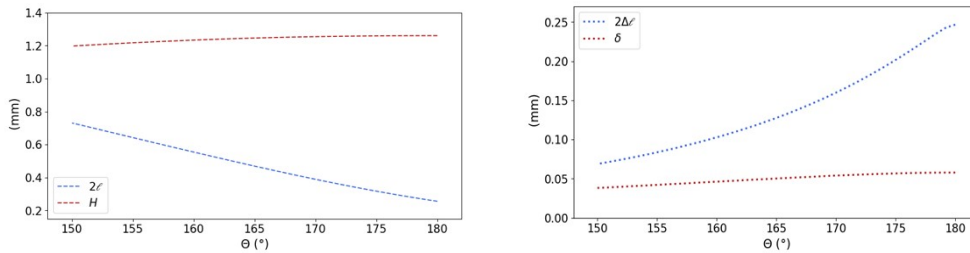


Figure S3. Effect of contact angle and gravity on the characteristic sizes of a non-wetting drop. Distances are deduced from the resolution of the Laplace equation for a volume of liquid $\Omega = 1.2 \mu\text{L}$. **a.** Contact size $2l$ and drop height H as a function of θ . l is the radius of the drop/substrate contact, where contact is the flat zone at the base of the drop due to wetting and/or gravity, as defined in figures 1a and 1b of the accompanying paper. We note that the distance l has a much higher sensitivity to the value of θ than the height H , justifying the use of this parameter as a tool for measuring the contact angle. **b.** Influence of gravity: we plot the sagging δ of the drop due to gravity (see figure 1c) and the difference Δl of contact size between a drop with $g = 0$ and $g = 10 \text{ m/s}^2$, also visible in figure 1c. While δ hardly varies with θ , the influence of gravity on the contact size is all the more significant since the contact angle is high. In summary, this figure emphasizes why l is a relevant parameter to measure high contact angles.

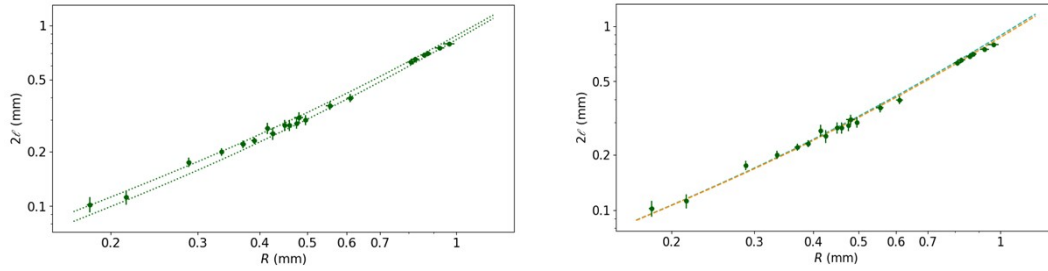


Figure S4. Accuracy of our measurements of high angles. We plot the measured contact size $2l$ as a function of the drop radius R , in a wide range of pearl volumes (factor larger than 100). Data is that plotted in figure 2 of the accompanying paper (green data), to which we superimpose the contact size calculated after solving the Laplace equation. **a.** θ is treated as an adjustable parameter and both dotted lines show the extreme values that fit the data, namely $\theta = 164.5^\circ$ (top curve) and $\theta = 166.5^\circ$ (bottom curve). Hence, we deduce an angle $\theta = 165.5^\circ$ with an accuracy of $\pm 1^\circ$. This accuracy defines the size of the error bars in the accompanying paper. **b.** For the same data, the dashed lines are fits obtained after integrating the Laplace equation for $\theta = 165.5^\circ$ and a capillary length $\kappa^{-1} = (\gamma(T)/\rho(T)g)^{1/2}$ of either 2.65 mm or 2.53 mm, which respectively correspond to a temperature $T = 50^\circ\text{C}$ (orange line) and $T = 90^\circ\text{C}$ (blue line). We barely distinguish the two curves, which justifies our choice of a constant $\kappa^{-1} (= 2.65 \text{ mm})$ in our fits, regardless of temperature.

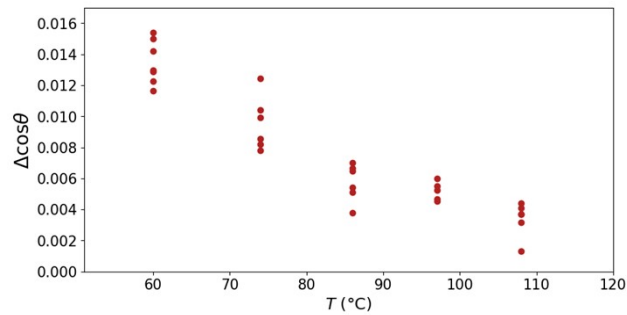


Figure S5. The measurement of contact angles (figure 4 of the accompanying paper) is complemented by determining the value of the contact angle hysteresis $\Delta\cos\theta$, which we plot as a function of the substrate temperature T . A millimetric drop is placed on the heated Glaco-coated material tilted until the drop departs. At this angle α , Furrmidge's formula expresses the balance of the weight $\rho g \Omega \sin\alpha$ with the sticking hysteretic force $\pi l \gamma \Delta\cos\theta$, which yields the quantity $\Delta\cos\theta$. For each tested temperature, we perform 5 or 6 experiments and so access the dispersity of our measurements. We consider in Furrmidge's equation the value for ρ and γ at each temperature. It is observed that the sticking parameter $\Delta\cos\theta$ is highly reduced, by a factor of order 4, when increasing temperature, a logical trend since sticking must disappear at the Leidenfrost point.

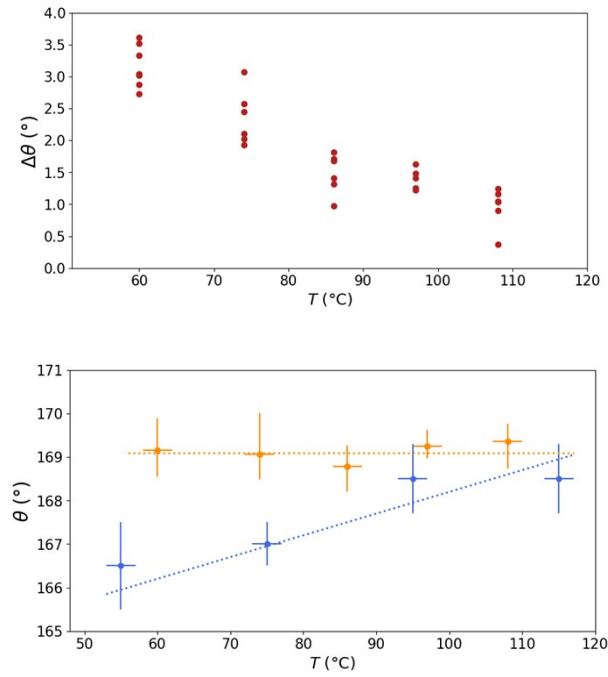


Figure S6. From figure S5 and from the value of the receding contact angle (blue data in figure 4a), we can deduce both $\Delta\theta$, the difference between advancing and receding angles on our super-hydrophobic samples, and θ_a , the advancing angle (second graph, where it is shown in orange while the receding angle θ_r is in blue). The advancing angle is found to be independent of temperature (within the error bars arising from the dispersity in figure S5), while the average receding angle increases with temperature (figure 4a in the accompanying paper). This qualitatively confirms our description: water on a warmer substrate tends to depin from the sites on which it sticks, since the production of vapor lowers the fraction of solid contacting the liquid (figure 4b) and thus impacts the receding angle responsible for the drop adhesion.